LaT-PFN: A Joint Embedding Predictive Architecture for In-context Time-series Forecasting

Stijn Verdenius[*]
WAIR, Amsterdam
stijn@wairforretail.com

Andrea Zerio[*]
WAIR, Amsterdam
andrea@wairforretail.com

Roy L.M. Wang
WAIR, Amsterdam
roy@wairforretail.com

Abstract

We introduce LatentTimePFN (LaT-PFN), a foundational Time Series model with a strong embedding space that enables zero-shot forecasting. To achieve this, we perform in-context learning in latent space utilizing a novel integration of the Prior-data Fitted Networks (PFN) and Joint Embedding Predictive Architecture (JEPA) frameworks. We leverage the JEPA framework to create a prediction-optimized latent representation of the underlying stochastic process that generates time series and combines it with contextual learning, using a PFN. Furthermore, we improve on preceding works by utilizing related time series as a context and introducing an abstract time axis. This drastically reduces training time and increases the versatility of the model by allowing any time granularity and forecast horizon. We show that this results in superior zero-shot predictions compared to established baselines. We also demonstrate our latent space produces informative embeddings of both individual time steps and fixed-length summaries of entire series. Finally, we observe the emergence of multi-step patch embeddings without explicit training, suggesting the model actively learns discrete tokens that encode local structures in the data, analogous to vision transformers.

1   Introduction

Time series forecasting is a fundamental task ubiquitous to various domains, ranging from finance [48, 34] to healthcare [32, 28], retail [24, 55], logistics [13] and beyond. Traditional approaches, both statistical [25, 14, 51] and deep-learning-based [47, 49], are frequently incapable of zero-shot forecasting [43] as they require training for each new dataset, limiting generalization capabilities.

In this paper, we introduce LatentTimePFN (LaT-PFN), a foundational Time Series model designed to address *zero-shot forecasting* by combining the Prior-data Fitted Networks (PFN) and Joint Embedding Predictive Architecture (JEPA) frameworks. LaT-PFN is trained exclusively on a novel synthetic data generation method, allowing us to encode expert knowledge directly in the training data. Furthermore, LaT-PFN learns to perform in-context learning in latent space by approximating the Posterior Predictive Distribution (PPD). We implement this meta-learning approach by enabling the model to learn zero-shot forecasting at test time, with user-provided time series functioning as exemplary context. We train LaT-PFN using an *abstract time dimension*, which consolidates a wider range of time-frequency patterns, facilitating meta-learning. Additionally, this improves the model's versatility and accuracy, whilst significantly reducing computational requirements. Following the JEPA methodology, LaT-PFN separates predicting and decoding, which are optimized independently. As such, LaT-PFN is trained to predict the next latent state and exploits a system identification loss as a regularization term, to independently improve the quality of its embedding space.

---

[*]Equal contributions

Our model demonstrates superior zero-shot prediction performance compared to baselines [10, 17, 51, 63], showcasing its effectiveness in handling unseen distributions. Additionally, LaT-PFN produces informative embeddings, demonstrating a comprehensive understanding of time series. Finally, we observe the emergence of multi-step patch embeddings without explicit training, suggesting that LaT-PFN actively learns discrete tokens encoding local structures in the data, reminiscent of vision transformers [18]. Our contributions are as follows:

- We introduce a novel architecture, LaT-PFN, which introduces a combination of the PFN and JEPA frameworks for zero-shot predictions of univariate time series in latent space.
- We introduce a novel synthetic prior for simulating context-aware time series data. Specifically, our prior allows for the creation of abstract-time synthetic contexts, defined as collections of time series, similar enough to enable LaT-PFN to approximate the PPD.
- We demonstrate, through extensive experimentation across a variety of datasets, that LaT-PFN outperforms established baselines with limited training resources, on multiple tasks.
- Finally, we offer an extensive analysis of the model's embedding space. This becomes particularly relevant as we notice the emergence of patch-like embeddings, without explicit training. We speculate this may be analogous to Vision Transformers (ViT) [18] and offer evidence it may even amount to a rudimentary time-series-specific corpus.

2 Background

2.1 PFN: Prior-data Fitted Networks

The Prior-data fitted Networks (PFN) methodology [41], is a meta-learning framework that explicitly trains a model for in-context learning. This is achieved through a neural network that approximates the posterior predictive distribution (PPD), thereby approximating Bayesian Inference. This requires a large volume of data, exhibiting a variety of related distributions. To facilitate this, the PFN trains on synthetic data generated by a simulation, whose parameters are sampled from a user-defined prior distribution $Pr(\psi)$. This allows developers to explicitly encode expert knowledge on the family of datasets Ψ that the PFN is trained on, rather than relying on implicitly encoding specialized knowledge in the model's architecture [41].

The PPD is typically defined as the probability distribution $P(y_*|x_*, \mathcal{D})$, with $\mathcal{D} = \{(x_i, y_i)\}^N$ being a context dataset. The PFN framework works by approximating this distribution:

$$Q_\theta(y_*|x_*, \mathcal{D}_j) \approx P(y_*|x_*, \mathcal{D}) \quad \text{with} \quad \mathcal{D}_j \sim S(\mathcal{D}_j|\psi_j), \quad \psi_j \sim Pr(\psi)$$

Here Q is a transformer [54] parametrized by θ, $S(.)$ is a simulation engine, and $Pr(.)$ is a prior distribution over instances of the simulation parameters $\psi \in \Psi$. Examples of the relation between features and targets are provided by the tuples (x_i, y_i) within $\mathcal{D}$, which are then passed through a transformer encoder [54]. The held-out features x_* are passed through the decoder, with a diagonal-only (independent) target mask, allowing only attention over the encoder context (Figure 1). Finally, a head and a cross-entropy loss are applied. The network Q is trained to perform meta-learning on any dataset $\mathcal{D}_j$ [41]. The authors prove that this is a valid approximation to the PPD – see Appendix B. Since its introduction, others have applied the PFN framework to various tasks [29, 17, 4, 23]. Notably, TabPFN [29] solves small tabular

Figure 1: PFN attention [41]

datasets, zero-shot. Additionally, ForecastPFN [17] introduced this methodology to time-series forecasting thanks to a novel synthetic prior.
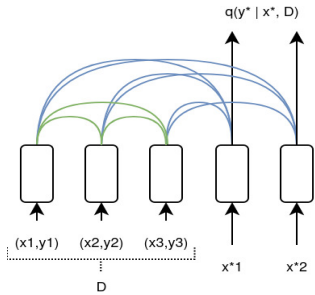
2.2 JEPA: Joint Embedding Predictive Architecture

The Joint Embedding Predictive Architecture (JEPA) [35] framework aims to create strong embeddings of any modality, to efficiently handle complex relationships within data. The key concept is to predict state transitions $S_t \rightarrow S_{t+1}$ fully in *latent space*, in order to create

embeddings that are not burdened by unnecessary detail. Figure 2 illustrates the core components, which define a sequence of transformations aimed at processing inputs within latent space. Initially, an input embedder $\bar{x} = E_x(x)$ converts the input into latent space.
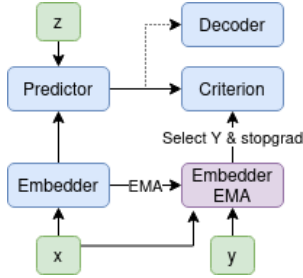

Figure 2: JEPA [35]

This is followed by a predictor $\hat{\bar{y}} = P(\bar{x}, z)$ which estimates the next latent state, using the transformed input and a variable z, intended to capture relationships not observable in the data space. A target embedder $\bar{y} = E_y(x, y)$ then maps the target, taking into account both x, y and their the relationship. A criterion, typically a Mean Squared Error (MSE) loss $C(\hat{\bar{y}}, \bar{y})$, evaluates the latent prediction. Finally, a generative decoder, $\hat{y} = D(\hat{\bar{y}})$, decodes the latent representations back to the data space.

The JEPA framework has since been applied to image and video data [5, 6]. The target encoder $y_L = E_y(x, y)$ is updated as an exponential moving average (EMA) of the input encoder E_x and followed by a stop gradient, preventing collapse by learning an identity mapping [35, 5]. Other JEPA works include Motion [7], Audio [22], Point-cloud [46] and EEG transfer [27].

3 Methodology

To the best of our knowledge, this work pioneers bringing energy-based JEPA [35] to time series forecasting, as well as combining it with the probabilistic PFN framework [41]. Initially, this integration may appear unconventional; however, we contend that these methodologies are complementary to this modality. JEPA separates concerns of predicting and decoding. This creates an embedding space more suited to the time series modality, which is inherently stochastic. LaT-PFN can thereby explicate latent patterns representing the underlying stochastic process, prioritizing inherent predictability. However, without in-context learning, univariate time series often still lack sufficient predictive power. The context provides samples of the underlying process, enhancing predictability through contextual learning. This is particularly important for time series datasets affected by cold-start and non-stationary issues. For example, one can imagine two series with identical histories but distinct target completions; a context then provides the additional information for extrapolation.

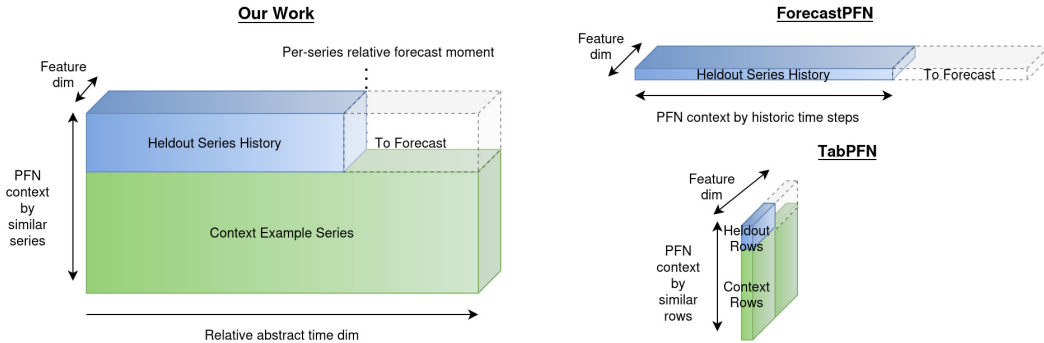### 3.1 Problem Statement

Figure 3: Problem statement of a time series forecasting PFN

Starting with a common definition of time series forecasting (TSF), we seek to derive a formulation of TSF for Bayesian Inference. In this work we consider a single supervised TSF problem $P(y|x)$ as predicting future values $y = v_{t+1:H} = [v_{t+1}, \ldots, v_H]$ from timestep t until horizon H, conditioned on the history $x = v_{0:t} = [v_0, \ldots, v_t]$. It follows that the PPD for this problem is defined as:

$$P(y_*|x_*, \mathcal{D}) = P(v_{*,t+1:H} \mid v_{*,0:t}, \{(x_i, y_i)\}^N), \quad (x_i, y_i) = (v_{i,0:t}, v_{i,t+1:H})$$

Where $\mathcal{D}$ is a context dataset with N examples, for $\mathcal{D} \in \mathbb{R}^{N \times S \times F}$, sequence dimension S, example dimension N and features F. This differs from the ForecastPFN formulation, which defines the

context $\mathcal{D} \in \mathbb{R}^{S \times F}$ as simply the history of the target time series [17]. This interpretation, although elegant, does not allow a context for the TSF task definition and is simply a regular forecasting task with simulated data. See Figure 3 for a visualization.

To complement this notation, let $\bar{x} = \bar{v}_{0:t}$ and latent target $\bar{y} = \bar{v}_{t+1:H}$ be the embedded versions of history $x = v_{0:t}$ and target $y = v_{t+1:H}$ respectively. Similarly, let $\hat{\bar{y}} = \hat{\bar{v}}_{t+1:H}$ be the latent forecast, and $\hat{y} = \hat{v}_{t+1:H}$ be the forecast in data space.

3.2 Abstract Time Dimension

Unlike [17], instead of using absolute time units (year, month, etc.), we map time to a fixed abstract interval $T_0 : T_H$ relative to the forecast start t of each series, with a variable sampling rate – while ensuring the absence of any data leakage. This allows us to map context time series and past segments of the held-out series onto the same interval, independent of their actual place in history. The approach aligns well with the idea of using simulated data to learn Bayesian inference, as it creates a universal and consistent time dimension in which the model can more readily learn general temporal patterns. Furthermore, reducing the number of temporal degrees of freedom that require training, leads to a more efficient convergence and significantly decreases the computational demands for training.

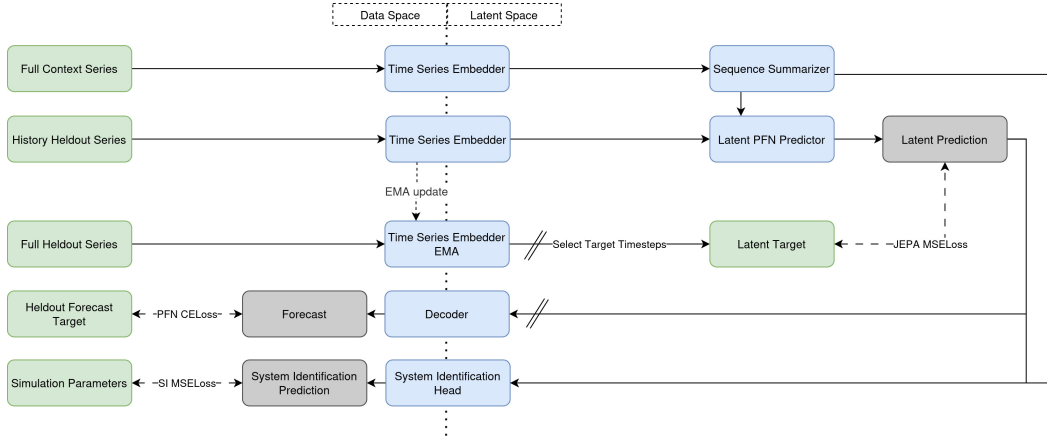## 3.3 An Architecture for Latent In-context Forecasting

Figure 4: The LaT-PFN Architecture. The context is embedded in fixed-length series-vectors. These are fed into the PFN Predictor transformer, with the embedded held-out history prompts, using cross-attention. The latent predictions are compared to the latent target, then decoded with a stopgradient, and compared to real targets. Finally, we apply a supervised regularisation on simulation parameters.
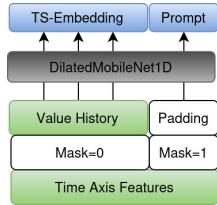

Figure 5: Production of embeddings and prompts by masking and selection

Embedder The embedder $E(.)$ is an eight-layer dilated Mobilenet1D [30]. We empirically found convolutions to be superior to attention over the sequence dimension, in line with [63, 38]. The component is responsible for feature extraction along the sequence dimension. First, we create the context embeddings $\bar{\mathcal{D}}$ and the latent target $\bar{y}$ with time T and value V features. For the latent target specifically, we use an EMA of the embedder parameters, apply a stop gradient, and select only the future timesteps:

$$\bar{\mathcal{D}} = E_\theta(\mathcal{D})$$

$$\bar{y} = Select_{t+1:H}\big[\,StopGrad\big(E_{\theta_{EMA}}(x, y)\big)\,\big]$$

Next, we create the held-out embeddings $\bar{x}$ and the prompt $\bar{z}$:

$$\bar{x}, \bar{z} = E_\theta(x)$$

To avoid introducing forward-looking values, we apply padding and masking to the input features. The prompt is therefore a function of the historical values and the entire time axis (including the horizon). See Figure 5 for an illustration of the aforementioned process.

4

Predictor The predictor $PFN_\theta(.)$ forecasts the next latent state, given the prompt and context. We apply learned average pooling AVG_θ over the sequence dimension of the embedded context $\bar{\mathcal{D}}$, by cross-attention with a learned vector $\vec{q} \in \theta$. These are then provided to the encoder of the latent PFN predictor 4, with self-attention over the examples dimension.

$$\bar{\eta} = AVG_\theta(\bar{\mathcal{D}})$$

In order to apply 2D attention over the held-out series, we flatten the examples dimension N and sequence dimension S of the prompt $\bar{z}$. Next, we pass it to the decoder, whilst ensuring adjacent sequences from held-out series are not dependent on sharing information.

$$M = diag(1)^{N \cdot S \times N \cdot S}, \quad \hat{\bar{y}} = PFN_\theta(\bar{z}, \bar{\eta}, M), \quad \mathcal{L}_{\text{latent}} = \frac{1}{n} \sum^{n} (\hat{\bar{y}} - \bar{y})^2$$

This is achieved by the diagonal-only mask M, which we adopt from the original PFN formulation [41]. Consequently, we stay true to the design from Figure 1.

Decoder The decoder $D_\theta(.)$ is a three-layer feedforward network, trained with independent gradients in alignment with the JEPA methodology [35, 5, 6]. We empirically found this to be critical for generating stable embeddings. The decoder utilizes a cross-entropy loss (see Appendix B) to define a categorical distribution over 100 segmented bins of the output space, incorporating label smoothing of 0.01 [50]. This is made feasible by casting the values V to an abstract space through z-normalizing with 2-std. By working in a value-abstract space, the decoder yields an output without making any assumptions on the target distribution – adhering closely to the PFN formulation [41].

$$\hat{y} = D_\theta(StopGrad(\hat{\bar{y}})), \quad \mathcal{L}_{\text{decoder}} = \mathbb{E}_{p(y)} \log p(\hat{y} \mid \hat{\bar{y}})$$

System Identification Head Inspired by Sim2Real research (e.g. [62]), we add a regularization term, to encourage consistency between history and forecast. This component processes the summarised vectors of both context and predicted held-out series, to identify the simulation parameters that generated the context $\mathcal{D}$. This approach further supervises the latent space, directing it to the underlying characteristics of the simulation, such as trend and seasonality. This, in turn, leads to improved forecasting capabilities and stabilizes training [35]. The latent embeddings and predictions are concatenated and averaged, then passed to a head $H_\theta(.)$ alongside the embedded context. $H_\theta(.)$ learns a multi-target regression towards unit-normalized simulation parameters.

$$\hat{y}_{\text{si}} = H_\theta(AVG_\theta(\hat{\bar{y}}, \bar{x}), \bar{C}), \quad \mathcal{L}_{\text{si}} = \frac{1}{n} \sum^{n} (\hat{y}_{\text{si}} - \psi_j)^2$$

Loss We define our loss as follows:

$$\mathcal{L} = \lambda_{\text{latent}} \mathcal{L}_{\text{latent}} + \lambda_{si} \mathcal{L}_{\text{si}} + \mathcal{L}_{\text{decoder}}, \quad \lambda_{\text{latent}} = 3.77e^{-3}, \quad \lambda_{si} = 1e^{-7}$$

The decoder is trained following a stop-gradient operation, ensuring one-way independence.

3.4 Context-aware Synthetic Prior with Triple Sampling

Following the PFN example [41, 17, 29], Lat-PFN was trained exclusively on synthetic data. For this work, we adopted and adjusted ForecastPFN's time series synthetic prior [17]. Like ForecastPFN, we set hyperprior parameters that govern sampling simulation parameters. Unlike ForecastPFN however, our context is defined not by the history of a single time series, but by a collection of example time series. Hence, for most simulation parameters, we introduce a context dimension by employing a three-step sampling strategy:

$$\alpha_c \sim \mathcal{U}(\alpha^*)$$
$$\mu_1, \mu_2 \sim \mathcal{U}(\alpha_c),$$
$$\psi_i \sim \mathcal{N}(\mu_1, \sigma^*), \quad \psi_j \sim \mathcal{N}(\mu_2, \sigma^*), \quad i, j \in [0, N]$$

Specifically, for any simulation parameter in ψ_i the procedure is defined as:

1. **Hyperprior Parameters** (α^*): Set the global limits for context synthesis.
2. **Context Parameters** (α_c): Ranges sampled uniformly from the hyperprior to define the limits within an individual context.
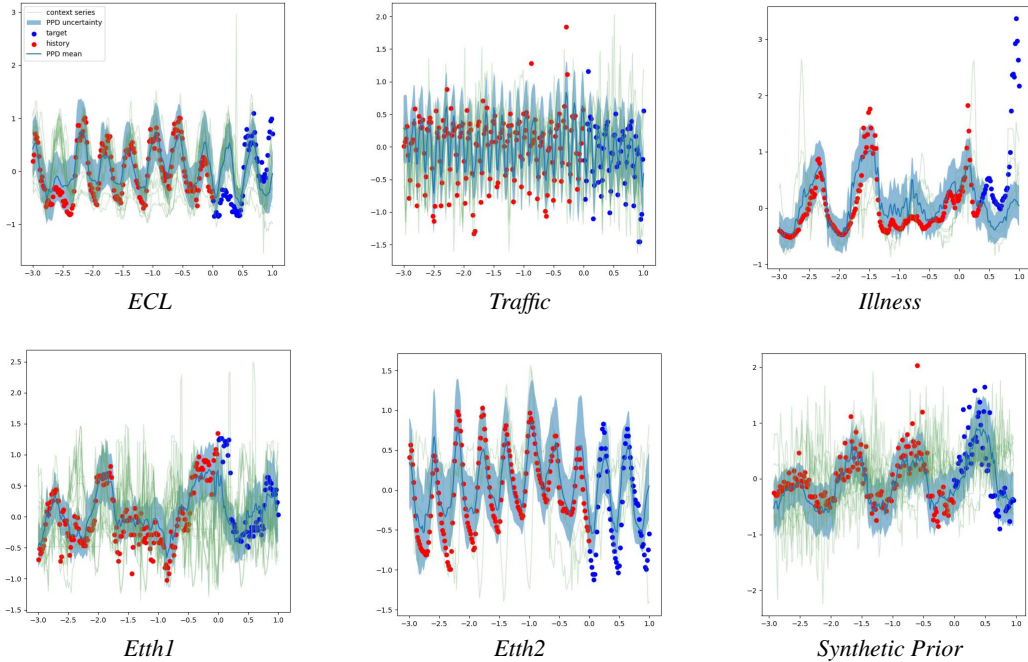
Figure 6: Decoded fits plotted on the target, with history and target in blue and red scatter respectively, as well as the PPD fore- and backcast mean as blue line with variance, and finally the input example context in green in the background. The fits demonstrate the predictions in latent space have picked up concepts such as seasonality and trend, making it easier to extrapolate after the forecast moment.

3. **Sub-context Parameters** (μ): Cluster centers as (μ_1, μ_2) sampled uniformly from the context range, are used to introduce contrast within a context and guide the model to recognize when a context example may be non-informative.

4. **Series Parameters** (ψ): Point estimates normally sampled using a fixed hyperprior variance σ^*, used as simulation parameters in $S(v_{i,0:T}|\psi_i)$ to generate individual training data series.

This approach ensures balance in inter- and intra-context variance, promoting coherence without trivializing the series and enhancing the model's ability to generalize in a zero-shot setting. A full description of the synthetic prior and which parameters are used can be found in appendix C.1.

4 Experimental Setup and Training Details

Training   During training, we employ a linear warmup schedule for weight decay, and target encoder ema decay – in line with previous JEPA work [5, 6]. We trained the final model for 24 hours on a single NVIDIA A10G Tensor Core GPU – per seed. Additionally, we employ tuning on schedule parameters and μ-parametrization, which was essential for training stability [59]. For more training and tuning details, see Appendix C.

Metrics   We report the mean and error statistics of the zero-shot performance of multiple seeds. These are accuracy, MSE per time-step, and the cumulative relative root mean squared error (CR-RMSE). The latter is normalized by the cumulative target. We motivate choosing CRRMSE for being scale-invariant, and practical applicability in tasks such as sales forecasting.

Benchmarks & Context Curation   For real datasets, fixed sequence length contexts were provided to the model. These were mapped to an abstract interval and Z-normalized with 2-std using the history. Which samples to include as contexts is coined *Context Curation*, and is a process analogous to Prompt Engineering in Large Language Models (LLMs) [40, 56]. For details, see Appendix C.

Table 1: Forecasting scores (with std) for different time horizons. Results demonstrate a strong performance for all of the benchmarks from decoded latent predictions. For details see Appendix C

	ECL	ETTh1	ETTh2	Illness	Traffic
Mean Squared Error (MSE)					
Arima	0.44	**0.44**	**0.45**	0.50	0.25
ForecastPFN	1.16	0.84	0.74	3.05	0.24
FBProphet	0.61	0.98	0.67	0.96	0.29
LaT-PFN	**0.32** ± 4.0e-2	0.59 ± 3.0e-2	**0.45** ± 1.8e-2	**0.23** ± 2.3e-2	**0.23** ± 2.8e-2
Cumulative Relative Root Mean Squared Error (CRRMSE)					
Arima	5.83	4.93	4.74	5.02	2.68
ForecastPFN	11.39	7.07	6.66	15.6	4
FBProphet	5.75	8.33	6.42	7.79	3.34
LaT-PFN	**4.03** ± 2.4e-1	**4.75** ± 2.1e-1	**3.95** ± 1.5e-1	**3.11** ± 1.8e-1	**2.01** ± 2.0e-1

Baselines We selected FBProphet [51], ARIMA [10], and ForecastPFN [17] as forecasting baselines, all of which have open-source codebases. We compared against TS2Vec, in a downstream classification task, [63] to evaluate the quality of the embedding space. We use the original authors' codebase and either download the trained model weights or re-train, wherever applicable. Finally, all baselines are tuned, where applicable, and then evaluated on identical datasets. For more details on baselines, see Appendix C.

5 Results & Discussion

Forecasting We find that LaT-PFN exhibits strong, zero-shot forecasting performance across a wide variety of datasets, containing very different temporal patterns and levels of noise. We outline the results of the zero-shot forecasting experiments in Table 1. As can be observed, in nearly all cases LaT-PFN outperforms the baselines. Furthermore, we demonstrate visual curve-fits in Figure 6. Here we can see the model understands useful patterns from the context, such as trend and seasonality, and uses them to reach a good extrapolation for the held-out

Table 2: Overall accuracy of UCR datasets, by fitting SVM on top of fixed-length summary embeddings [20]. Per-dataset scores are in Appendix E.

	training budget	accuracy
TS2Vec	finetuned	45.7%
LaT-PFN	zero-shot	**51.1%**

targets. This suggests that LaT-PFN is inherently strong at generalizing across distributions for zero-shot forecasting, which makes it widely applicable for downstream tasks.
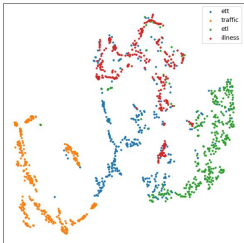

Figure 7: T-SNE [53] of fixed-length embeddings by dataset

Next, we investigate the importance of the context by evaluating the uplift in performance on a synthetic validation set, for different context sizes. We chose to carry out this experiment on simulated data to guarantee a control environment. The result is visualized in Figure 8, which shows a clear correlation between performance and context size. More interestingly, this pattern persists even beyond the original context size of the model during training (represented by the vertical dotted line). This validates our assumption that the key to carrying out in-context learning for zero-shot forecasting is to provide a rich and substantial set of examples. This can be especially impactful when applied in a production setting with an abundance of example series, such as sales forecasting.

Classification We evaluate the quality of LaT-PFN's embedding space by introducing a second downstream task, namely time series classification on the 129 multi-domain UCR datasets. We compare our model to TS2Vec, a state-of-the-art universal representation learning framework for time series [63]. We train TS2Vec on the UCR datasets, then fit Support Vector Machines (SVM) [8] on their embedding space. We compare this to an SVM fitted on the fixed-length summary embeddings of a frozen LaT-PFN, trained on synthetic data only. As is
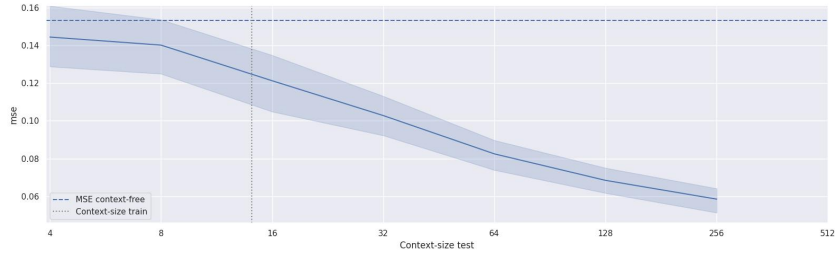
Figure 8: Extrapolating evaluation context generalizes beyond training context size
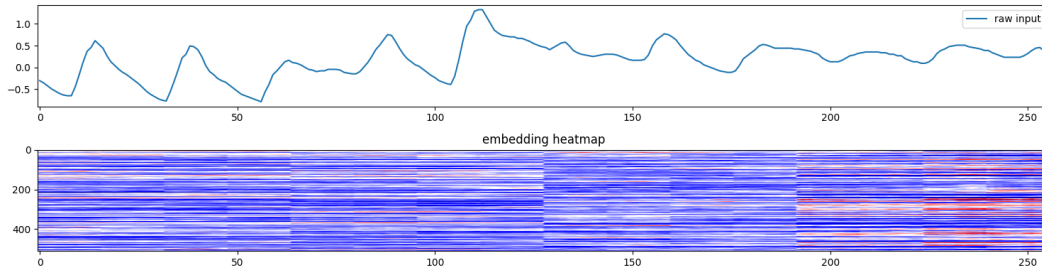

Figure 9: Embeddings per-timestep show patch-like behavior. More in Appendix D

evident in the results reported in Table 2, LaT-PFN outperforms TS2Vec across the entire benchmark of datasets. See Appendix E for individual dataset scores.

We argue these results may be due to bias introduced by time series-specific heuristics and contrastive positive pair selection, both of which TS2Vec and similar methods rely heavily upon [63, 60]. By contrast, LaT-PFN independently discovers the most representative embedding space in which self-supervised learning is most optimal. Furthermore, TS2Vec is trained on the datasets it is evaluated on. This may traditionally be thought of as an advantage. Yet, often these datasets are small and lack variety, increasing the risk of out-of-distribution data in the test set. On the other hand, LatPFN's prior ensures a wider variety of contexts, whilst adapting to the specific context during test time.

Exploring the Embedding Space We carry out a qualitative analysis of the latent space generated by LaT-PFN. When analyzing the fixed-length summary embeddings after dimensionality reduction, we observe a clear separation in clusters by dataset – see Figure 7. This suggests that LaT-PFN picks up distributional differences between these domains, making these fixed-length summary embeddings useful for search, classification and other downstream applications.

Interestingly we can observe the emergence of distinct, regular, and discrete patch-like tokens in the heatmaps of the embedding space. An example of this is visualized in Figure 9. Whilst not always humanly interpretable, discernible patterns often emerge from a closer analysis of these patches. For in-

Figure 10: Found patches (red) and top-3 closest matches (blue)

stance, Figure 10 plots some examples in the data space, alongside their closest matches when taking the L_2-distance between the average patch-embedding. We can observe that these are visually related and seem to describe specific local features. This presents similarities to the patch-like processing of visual "tokens" in Vision Transformers (ViT) and their approach to high-level feature representation [18]. LaT-PFN, however, appears to have learned these tokens independently, without the need to outright encode this pattern in the model's architecture.

Finally, after applying dimensionality reduction to the set of patch embeddings (Figure 11), we notice the clear emergence of a few clusters. Given the aforementioned similarity between shapes of patches in data space with similar token embeddings, we speculate these could be a latent vocabulary that has been independently learned by the model, consisting of common "words" amongst multi-domain

8

series. This would once more validate our core assumption that, despite time series data often being perceived as highly domain-dependant, there is in fact enough commonality to warrant the use of meta-learning approaches to create foundational models for this data modality.

6 Related Work

For time series forecasting, focus has recently shifted from statistical models such as ARIMA [10], ES [25] and FBProphet [51] towards deep learning. Early pioneers are DeepAR [47] and hybrid methods [49]. Subsequently, N-Beats [42], N-hits [12], Informer [65] and FEDformer [66], combine classical with deep learning paradigms.

More recently, following the success of the NLP domain, many attempts have been made to leverage the transformer architecture [54] to create foundation models [9] for time series forecasting. The two main approaches for doing so can be categorized as; (a) re-purposing LLMs [26, 67, 31] and (b) training transformer models from scratch

Figure 11: DBScan [19] clustering of patches.

[17, 4, 57, 15, 61, 45]. By contrast, our research seeks to integrate representation- and in-context learning in time series forecasting, combining strong performance with a low computational budget.

Another approach altogether is to create embeddings and leave the downstream application to the discretion of end users. Notable are TS2Vec [63], TimeCLR [60], SimMTM [16] and TF-C [64]. These methods often rely heavily on expert heuristics, whereas our approach serves both as an embedder and a forecaster, instead leveraging a self-supervised latent space to drive predictions.
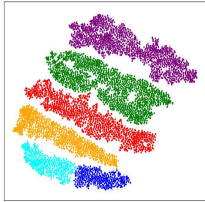
7 Limitations

The research presented has a few limitations. Firstly, the current framework is constrained to univariate series, limiting its applicability to multivariate scenarios. Similarly, this model has yet to prove effective in handling hierarchical, discrete, or zero-inflated series, which are often underrepresented in this research field. Defining appropriate synthetic priors could address this, which we leave to future work. Secondly, we observe a low level of standardization for time series deep learning research. Whilst we found an (over) abundance of standard datasets, we observed that data processing, and target and horizon selection are still arbitrary, reducing the comparability of results across studies. This is beyond the scope of this paper but may be addressed in future work. Finally, we designed our model to be highly adaptive to a given context. As a result, sub-optimal contexts can lead to variability in performance. We argue this is analogous to prompt engineering, which assigns this responsibility to the expert user. In future work, we hope to address this by exploring automated methods – via retrieval augmented generation (RAG) [37] or prompt tuning [36]. Addressing these points will be valuable for enhancing the model's versatility.

8 Conclusion

In this paper, we proposed LaT-PFN, a novel architecture for zero-shot univariate time series forecasting. The model integrates both the PFN and JEPA architecture to allow for in-context learning in latent space. LaT-PFN is trained exclusively on synthetic data, for which we define a novel prior. Combined with an abstract time dimension, this makes our model extremely versatile and able to achieve strong forecasting results across different data distributions, time granularities, and forecast horizons. Finally, its strong embedding space exhibits interesting emergent qualities, such as the development of patch-like tokens that resemble a corpus of time series features. This makes LaT-PFN ideal for supporting transfer learning on downstream models.

Acknowledgments and Disclosure of Funding

References

[1] URL `https://gis.cdc.gov/grasp/fluview/fluportaldashboard.html`.

[2] Abacusai. Abacusai/forecastpfn. URL `https://github.com/abacusai/ForecastPFN`.

[3] T. Akiba, S. Sano, T. Yanase, T. Ohta, and M. Koyama. Optuna: A next-generation hyperparameter optimization framework. In *Proceedings of the 25th ACM SIGKDD International Conference on Knowledge Discovery and Data Mining*, 2019.

[4] A. F. Ansari, L. Stella, C. Turkmen, X. Zhang, P. Mercado, H. Shen, O. Shchur, S. S. Rangapuram, S. P. Arango, S. Kapoor, et al. Chronos: Learning the language of time series. *arXiv preprint arXiv:2403.07815*, 2024.

[5] M. Assran, Q. Duval, I. Misra, P. Bojanowski, P. Vincent, M. Rabbat, Y. LeCun, and N. Ballas. Self-supervised learning from images with a joint-embedding predictive architecture. In *Proceedings of the IEEE/CVF Conference on Computer Vision and Pattern Recognition*, pages 15619–15629, 2023.

[6] A. Bardes, Q. Garrido, J. Ponce, X. Chen, M. Rabbat, Y. LeCun, M. Assran, and N. Ballas. V-jepa: Latent video prediction for visual representation learning. 2023.

[7] A. Bardes, J. Ponce, and Y. LeCun. Mc-jepa: A joint-embedding predictive architecture for self-supervised learning of motion and content features. *arXiv preprint arXiv:2307.12698*, 2023.

[8] C. M. Bishop and N. M. Nasrabadi. *Pattern recognition and machine learning*, volume 4. Springer, 2006.

[9] R. Bommasani, D. A. Hudson, E. Adeli, R. Altman, S. Arora, S. von Arx, M. S. Bernstein, J. Bohg, A. Bosselut, E. Brunskill, et al. On the opportunities and risks of foundation models. *arXiv preprint arXiv:2108.07258*, 2021.

[10] G. E. Box, G. M. Jenkins, G. C. Reinsel, and G. M. Ljung. *Time series analysis: forecasting and control*. John Wiley & Sons, 2015.

[11] Caltrans PeMS. Caltrans performance measurement system (pems), US DOT, 2021.

[12] C. Challu, K. G. Olivares, B. N. Oreshkin, F. G. Ramirez, M. M. Canseco, and A. Dubrawski. Nhits: Neural hierarchical interpolation for time series forecasting. In *Proceedings of the AAAI Conference on Artificial Intelligence*, volume 37, pages 6989–6997, 2023.

[13] H. K. Chan, S. Xu, and X. Qi. A comparison of time series methods for forecasting container throughput. *International journal of logistics research and applications*, 22(3):294–303, 2019.

[14] J. Contreras, R. Espinola, F. J. Nogales, and A. J. Conejo. Arima models to predict next-day electricity prices. *IEEE transactions on power systems*, 18(3):1014–1020, 2003.

[15] A. Das, W. Kong, R. Sen, and Y. Zhou. A decoder-only foundation model for time-series forecasting. *arXiv preprint arXiv:2310.10688*, 2023.

[16] J. Dong, H. Wu, H. Zhang, L. Zhang, J. Wang, and M. Long. Simmtm: A simple pre-training framework for masked time-series modeling. *Advances in Neural Information Processing Systems*, 36, 2024.

[17] S. Dooley, G. S. Khurana, C. Mohapatra, S. Naidu, and C. White. Forecastpfn: Synthetically-trained zero-shot forecasting. *arXiv preprint arXiv:2311.01933*, 2023.

[18] A. Dosovitskiy, L. Beyer, A. Kolesnikov, D. Weissenborn, X. Zhai, T. Unterthiner, M. Dehghani, M. Minderer, G. Heigold, S. Gelly, et al. An image is worth 16x16 words: Transformers for image recognition at scale. *arXiv preprint arXiv:2010.11929*, 2020.

[19] M. Ester, H.-P. Kriegel, J. Sander, X. Xu, et al. A density-based algorithm for discovering clusters in large spatial databases with noise. In *kdd*, volume 96, pages 226–231, 1996.

[20] D. et al. The ucr time series classification archive, 2018. URL `https://www.cs.ucr.edu/~eamonn/time_series_data_2018/`. Accessed: 2024-05-14.

[21] Facebook. Facebook/prophet: Tool for producing high quality forecasts for time series data that has multiple seasonality with linear or non-linear growth. URL `https://github.com/facebook/prophet`.

[22] Z. Fei, M. Fan, and J. Huang. A-jepa: Joint-embedding predictive architecture can listen. *arXiv preprint arXiv:2311.15830*, 2023.

[23] B. Feuer, N. Cohen, and C. Hegde. Scaling tabpfn: Sketching and feature selection for tabular prior-data fitted networks. In *NeurIPS 2023 Second Table Representation Learning Workshop*, 2023.

[24] R. Fildes, S. Ma, and S. Kolassa. Retail forecasting: Research and practice. *International Journal of Forecasting*, 38(4):1283–1318, 2022.

[25] E. S. Gardner Jr. Exponential smoothing: The state of the art. *Journal of forecasting*, 4(1):1–28, 1985.

[26] N. Gruver, M. Finzi, S. Qiu, and A. G. Wilson. Large language models are zero-shot time series forecasters. *Advances in Neural Information Processing Systems*, 36, 2024.

[27] P. Guetschel, T. Moreau, and M. Tangermann. S-jepa: towards seamless cross-dataset transfer through dynamic spatial attention. *arXiv preprint arXiv:2403.11772*, 2024.

[28] H. Harutyunyan, H. Khachatrian, D. C. Kale, G. Ver Steeg, and A. Galstyan. Multitask learning and benchmarking with clinical time series data. *Scientific data*, 6(1):96, 2019.

[29] N. Hollmann, S. Müller, K. Eggensperger, and F. Hutter. Tabpfn: A transformer that solves small tabular classification problems in a second. In *The Eleventh International Conference on Learning Representations*, 2022.

[30] A. G. Howard, M. Zhu, B. Chen, D. Kalenichenko, W. Wang, T. Weyand, M. Andreetto, and H. Adam. Mobilenets: Efficient convolutional neural networks for mobile vision applications. *arXiv preprint arXiv:1704.04861*, 2017.

[31] M. Jin, S. Wang, L. Ma, Z. Chu, J. Y. Zhang, X. Shi, P.-Y. Chen, Y. Liang, Y.-F. Li, S. Pan, et al. Time-llm: Time series forecasting by reprogramming large language models. *arXiv preprint arXiv:2310.01728*, 2023.

[32] S. Kaushik, A. Choudhury, P. K. Sheron, N. Dasgupta, S. Natarajan, L. A. Pickett, and V. Dutt. Ai in healthcare: time-series forecasting using statistical, neural, and ensemble architectures. *Frontiers in big data*, 3:4, 2020.

[33] D. P. Kingma and J. Ba. Adam: A method for stochastic optimization. *arXiv preprint arXiv:1412.6980*, 2014.

[34] B. Krollner, B. Vanstone, and G. Finnie. Financial time series forecasting with machine learning techniques: A survey. In *European Symposium on Artificial Neural Networks: Computational Intelligence and Machine Learning*, pages 25–30, 2010.

[35] Y. LeCun. A path towards autonomous machine intelligence version 0.9. 2, 2022-06-27. *Open Review*, 62 (1), 2022.

[36] B. Lester, R. Al-Rfou, and N. Constant. The power of scale for parameter-efficient prompt tuning. *arXiv preprint arXiv:2104.08691*, 2021.

[37] P. Lewis, E. Perez, A. Piktus, F. Petroni, V. Karpukhin, N. Goyal, H. Küttler, M. Lewis, W.-t. Yih, T. Rocktäschel, et al. Retrieval-augmented generation for knowledge-intensive nlp tasks. *Advances in Neural Information Processing Systems*, 33:9459–9474, 2020.

[38] Y. Liu, T. Hu, H. Zhang, H. Wu, S. Wang, L. Ma, and M. Long. itransformer: Inverted transformers are effective for time series forecasting. *arXiv preprint arXiv:2310.06625*, 2023.

[39] I. Loshchilov and F. Hutter. Decoupled weight decay regularization. *arXiv preprint arXiv:1711.05101*, 2017.

[40] G. Marvin, N. Hellen, D. Jjingo, and J. Nakatumba-Nabende. Prompt engineering in large language models. In *International Conference on Data Intelligence and Cognitive Informatics*, pages 387–402. Springer, 2023.

[41] S. Müller, N. Hollmann, S. P. Arango, J. Grabocka, and F. Hutter. Transformers can do bayesian inference. In *International Conference on Learning Representations*, 2021.

[42] B. N. Oreshkin, D. Carpov, N. Chapados, and Y. Bengio. N-beats: Neural basis expansion analysis for interpretable time series forecasting. *arXiv preprint arXiv:1905.10437*, 2019.

[43] B. N. Oreshkin, D. Carpov, N. Chapados, and Y. Bengio. Meta-learning framework with applications to zero-shot time-series forecasting. In *Proceedings of the AAAI Conference on Artificial Intelligence*, volume 35, pages 9242–9250, 2021.

[44] J. Perktold, S. Seabold, J. Taylor, and statsmodels developers. statsmodels.tsa.arima.model.arima — statsmodels 0.15.0 documentation, 2024. URL https://www.statsmodels.org/dev/generated/statsmodels.tsa.arima.model.ARIMA.html. Accessed: 2024-05-14.

[45] K. Rasul, A. Ashok, A. R. Williams, A. Khorasani, G. Adamopoulos, R. Bhagwatkar, M. Biloš, H. Ghonia, N. V. Hassen, A. Schneider, et al. Lag-llama: Towards foundation models for time series forecasting. *arXiv preprint arXiv:2310.08278*, 2023.

[46] A. Saito and J. Poovvancheri. Point-jepa: A joint embedding predictive architecture for self-supervised learning on point cloud. *arXiv preprint arXiv:2404.16432*, 2024.

[47] D. Salinas, V. Flunkert, and J. Gasthaus. Deepar: Probabilistic forecasting with autoregressive recurrent networks. *arXiv preprint arXiv:1704.04110*, 2017.

[48] O. B. Sezer, M. U. Gudelek, and A. M. Ozbayoglu. Financial time series forecasting with deep learning: A systematic literature review: 2005–2019. *Applied soft computing*, 90:106181, 2020.

[49] S. Smyl. A hybrid method of exponential smoothing and recurrent neural networks for time series forecasting. *International Journal of Forecasting*, 36(1):75–85, 2020.

[50] C. Szegedy, V. Vanhoucke, S. Ioffe, J. Shlens, and Z. Wojna. Rethinking the inception architecture for computer vision. In *Proceedings of the IEEE conference on computer vision and pattern recognition*, pages 2818–2826, 2016.

[51] S. J. Taylor and B. Letham. Forecasting at scale. *The American Statistician*, 72(1):37–45, 2018.

[52] A. Trindade. ElectricityLoadDiagrams20112014. UCI Machine Learning Repository, 2015. DOI: https://doi.org/10.24432/C58C86.

[53] L. Van der Maaten and G. Hinton. Visualizing data using t-sne. *Journal of machine learning research*, 9 (11), 2008.

[54] A. Vaswani, N. Shazeer, N. Parmar, J. Uszkoreit, L. Jones, A. N. Gomez, Ł. Kaiser, and I. Polosukhin. Attention is all you need. *Advances in neural information processing systems*, 30, 2017.

[55] K. Wanchoo. Retail demand forecasting: a comparison between deep neural network and gradient boosting method for univariate time series. In *2019 IEEE 5th International Conference for Convergence in Technology (I2CT)*, pages 1–5. IEEE, 2019.

[56] J. White, Q. Fu, S. Hays, M. Sandborn, C. Olea, H. Gilbert, A. Elnashar, J. Spencer-Smith, and D. C. Schmidt. A prompt pattern catalog to enhance prompt engineering with chatgpt. *arXiv preprint arXiv:2302.11382*, 2023.

[57] G. Woo, C. Liu, A. Kumar, C. Xiong, S. Savarese, and D. Sahoo. Unified training of universal time series forecasting transformers. *arXiv preprint arXiv:2402.02592*, 2024.

[58] H. Wu, J. Xu, J. Wang, and M. Long. Autoformer: Decomposition transformers with auto-correlation for long-term series forecasting. *Advances in neural information processing systems*, 34:22419–22430, 2021.

[59] G. Yang, E. J. Hu, I. Babuschkin, S. Sidor, X. Liu, D. Farhi, N. Ryder, J. Pachocki, W. Chen, and J. Gao. Tensor programs v: Tuning large neural networks via zero-shot hyperparameter transfer. *arXiv preprint arXiv:2203.03466*, 2022.

[60] X. Yang, Z. Zhang, and R. Cui. Timeclr: A self-supervised contrastive learning framework for univariate time series representation. *Knowledge-Based Systems*, 245:108606, 2022.

[61] C.-C. M. Yeh, X. Dai, H. Chen, Y. Zheng, Y. Fan, A. Der, V. Lai, Z. Zhuang, J. Wang, L. Wang, et al. Toward a foundation model for time series data. In *Proceedings of the 32nd ACM International Conference on Information and Knowledge Management*, pages 4400–4404, 2023.

[62] W. Yu, V. C. Kumar, G. Turk, and C. K. Liu. Sim-to-real transfer for biped locomotion. In *2019 ieee/rsj international conference on intelligent robots and systems (iros)*, pages 3503–3510. IEEE, 2019.

[63] Z. Yue, Y. Wang, J. Duan, T. Yang, C. Huang, Y. Tong, and B. Xu. Ts2vec: Towards universal representation of time series. In *Proceedings of the AAAI Conference on Artificial Intelligence*, volume 36, pages 8980–8987, 2022.

[64] X. Zhang, Z. Zhao, T. Tsiligkaridis, and M. Zitnik. Self-supervised contrastive pre-training for time series via time-frequency consistency. In S. Koyejo, S. Mohamed, A. Agarwal, D. Belgrave, K. Cho, and A. Oh, editors, *Advances in Neural Information Processing Systems*, volume 35, pages 3988–4003. Curran Associates, Inc., 2022. URL `https://proceedings.neurips.cc/paper_files/paper/2022/file/194b8dac525581c346e30a2cebe9a369-Paper-Conference.pdf`.

[65] H. Zhou, S. Zhang, J. Peng, S. Zhang, J. Li, H. Xiong, and W. Zhang. Informer: Beyond efficient transformer for long sequence time-series forecasting. In *Proceedings of the AAAI conference on artificial intelligence*, volume 35, pages 11106–11115, 2021.

[66] T. Zhou, Z. Ma, Q. Wen, X. Wang, L. Sun, and R. Jin. Fedformer: Frequency enhanced decomposed transformer for long-term series forecasting. In *International conference on machine learning*, pages 27268–27286. PMLR, 2022.

[67] T. Zhou, P. Niu, L. Sun, R. Jin, et al. One fits all: Power general time series analysis by pretrained lm. *Advances in neural information processing systems*, 36, 2024.

Appendix / supplemental material

A   Broader Societal Impacts

It is our belief that the work presented in this paper does not pose major negative societal risks. The model is trained exclusively on synthetic time series data, thus eliminating any risk related to data privacy, disinformation or consent. On the contrary, given how ubiquitous time series are in the real world, we hope that our model for zero-shot forecasting will provide a net benefit for society, for a few different reasons. Firstly, it is significantly more efficient to train than many of the baselines we evaluate against, as pointed out in Section 4. Secondly, as a zero-shot foundation model, it only requires training once, before being used out-of-the-box. Thirdly, many sectors in society could benefit from having improved forecasting abilities for assisting day-to-day decision-making. We hope this will result in widespread adoption of pre-trained models for forecasting tasks, thus improving industry effectiveness and reducing energy consumption and $CO2$ emissions.

B   Derivation PFN NLLLoss

This derivation shows how to approximate Bayesian Inference via a PFN. It is adapted from [41] and forms the justification of why using a simulation with a cross-entropy loss is an approximation of the PPD. Assume we want to approximate PPD $P(y|x,\mathcal{D})$ with network $Q(y|x,\mathcal{D})$. We start with the KL-divergence between the two and end up at entropy function $\boldsymbol{H}()$ and constant C. The latter does not depend on parameters θ and is dropped in optimisation.

$$
\begin{aligned}
&\mathbb{E}_{x,\mathcal{D}}\left[\ KL\big(P(y|x,\mathcal{D}),Q_\theta(y|x,\mathcal{D})\big)\ \right] \\
=\ &\mathbb{E}_{x,\mathcal{D}}\left[\ -\int_y P(y|x,\mathcal{D})\log\frac{Q_\theta(y|x,\mathcal{D})}{P(y|x,\mathcal{D})}\ \right] \\
=\ &\mathbb{E}_{x,\mathcal{D}}\left[\ -\int_y P(y|x,\mathcal{D})\log Q_\theta(y|x,\mathcal{D})\ \right]\ +\ \mathbb{E}_{x,\mathcal{D}}\left[\int_y P(y|x,\mathcal{D})\log P(y|x,\mathcal{D})\right] \\
=\ &\mathbb{E}_{x,\mathcal{D}}\left[\ \boldsymbol{H}\big(P(y|x,\mathcal{D}),Q_\theta(y|x,\mathcal{D})\big)\ \right]\ +\ C
\end{aligned}
$$

We can then integrate the PFN simulation by sampling the data from our prior:

$$
\begin{aligned}
\mathcal{L}\ =\ &\mathbb{E}_{\{(x,y)\cup\mathcal{D}\}\sim S(.|\psi)}\left[\ \boldsymbol{H}\big(P(y|x,\mathcal{D}),Q_\theta(y|x,\mathcal{D})\big)\ \right] \\
=\ &\mathbb{E}_{\{(x,y)\cup\mathcal{D}\}\sim S(.|\psi)}\left[\ -\sum_y P(y|x,\mathcal{D})\log Q_\theta(y|x,\mathcal{D})\big)\ \right]
\end{aligned}
$$

C   Reproducibility Details

This section is dedicated to providing comprehensive reproducibility details for the research presented in this document. By including this appendix, we aim to uphold transparency standards in research.

C.1   Exhaustive Description Synthesis Training Data

Following the example set by [17] we define a synthetic prior that leverages the underlying components of time series data, namely trend, seasonality, and noise. The trend parameter is made up of linear and exponential components; the seasonality parameter is made up of annual, monthly, and weekly components and the noise is derived from a Weibull distribution:

$$y_t = \psi(t) \cdot z_t = trend(t) \cdot seasonality(t) \cdot z_t$$

The linear and exponential trend components are defined by two constituent parts each: scaler and offset. The scaler m is a context-wide parameter, therefore we use triple sampling to generate them. The offset c is domain-specific, so we directly sample them, uniformly, from a range of hyperpriors. The formula for the trend component is the same as defined by [17]:

$$trend(t) = 1 + (m_{lin} \cdot t + c_{lin}) \cdot (m_{exp} \cdot c_t^{exp})$$

The seasonality parameters are all context-dependant, therefore we apply triple sampling to derive them. Additionally, we introduce a new parameter, δ to define the number of frequency features for each seasonality parameter. We use triple sampling for the seasonality parameters and direct univariate sampling for the δ parameter. The formulas have once again been adapted from [17]:

$$seasonal(t) = seasonal_{week}(t) \cdot seasonal_{month}(t) \cdot seasonal_{year}(t)$$

$$\delta_v \sim \mathcal{U}(\alpha_\delta^*)$$

$$seasonal_v(t) = 1 + m_v \sum_{f=1}^{\delta_v} \left[c_{f,v} \sin\left(2f\pi \frac{t}{p_v}\right) + d_{f,v} \cos\left(2f\pi \frac{t}{p_v}\right) \right]$$

$$v \in \{week, month, year\}$$

$$p_{week} = 7, \; p_{month} = 30.417, \; p_{year} = 30.417$$

$$c_v \sim \mathcal{N}\left(0, \frac{1}{|\delta_v|}\right), \; d_v \sim \mathcal{N}\left(0, \frac{1}{|\delta_v|}\right)$$

The noise component follows the definition laid out by [17], the only difference being that we sample a single k parameter per context, and use it in the Weibull distribution:

$$z = 1 + m_{noise}(z - \bar{z})$$

$$z \sim Weibull(1, k), \; \bar{z} = (\ln 2)^{1/k}, \; m_{noise} \in \{\mathcal{U}(0, 0.1), \mathcal{U}(0.2, 0.4), \mathcal{U}(0.6, 0.8)\}$$

Unlike [17], we train using an abstract time dimension. In order to include many different types of temporal patterns, we define a resolution parameter ρ, which determines how many points are represented per interval, for each individual time series. We define this as the relation between the sequence dimension and resolution parameter:

$$t = \frac{S}{\rho}$$

Finally, for the resolution and exponential-trend parameters, we obtain the context parameters α_c, described in Section 3.4, by sampling log-uniformly, due to the logarithmic nature of these components. Specifically, we guarantee a median sample value without having a forced symmetric range around that median value. To do so, we (a) define a mapping to log space, (b) sample uniformly, and (c) inverse the mapping after. The formula is as follows:

$$
\begin{aligned}
map(x, \kappa) &= log_2(x \cdot \kappa + 1) \\
map^{-1}(x, \kappa) &= \frac{2^x - 1}{\kappa} \\
\alpha_{c,mapped} &\sim \mathcal{U}\left(map(\alpha^*, \kappa)\right) \\
\alpha_c &= map^{-1}(\alpha_{c,mapped}, \kappa)
\end{aligned}
$$

For multiplier κ and function $map(.)$. Please see Table 3 for details on the multipliers and hyperpriors.

Table 3: Hyperpriors for Simulation Engine

Hyperparameter	Min Value	Max Value
Seasonality		
Annual Frequency Scale	-8.0	8.0
Monthly Frequency Scale	-4.0	4.0
Weekly Frequency Scale	-2.0	2.0
Variance	0.15	
Trend		
Linear	-0.015	0.015
Linear Variance	0.005	
Exponential	0.996	1.0016
Exponential Variance	0.001	
Exponential Multiplier $\kappa_{m_{exp}}$	507	
Noise		
Noise (k)	0.8	5
Resolution		
Resolution Min	0.1	1.0
Resolution Multiplier κ_ρ	53.6	
Offset		
Linear Offset	-1	2
Exponential Offset	-1	2
Harmonics		
$\delta_{\text{harmonics}}$	4	12

C.2 Baselines

Forecasting   For forecasting we use the following baselines:

- FBProphet [51], a common industry standard with respect to the type of univariate series we model. We use the publicly available repository [21] and manually tune the parameter `changepoint_prior_scale=1.0`.

- ARIMA [14], another classic baseline from the industry. We use the Statsmodel implementation [44] publicly available and pass the argument `order=(5, 1, 0)`.

- ForecastPFN [17] is a flexible in-context forcaster model and one of the inspirations for this work. We download their open-source repository available under Apache Licence 2.0 and trained model weights. We adopt their inference script to work in our repository. We have tried several data normalizations by hand to get the most out their model and picked the best one, which turned out to be Z-normalization with 2std – on top of the normalizations present in the repository already.

Classification   For classification we use the TS2Vec baseline [63], as it is a strong multi-purpose representation learner and also an inspiration for this work, although TS2Vec does not claim to implement zero-shot forecasting. They open-source their training code under the MIT Licence, so we train TS2Vec from scratch on the train splits of the UCR [20] archive, after which we evaluate on the corresponding test splits with the resulting frozen TS2Vec architecture

C.3 Benchmark Preprocessing

We use five datasets for our experiments, detailed in section 4. These are considered standard datasets for benchmarking the performance of time series forecasting models [43, 58, 65].

For each dataset, we create univariate time series out of each of the columns. Additionally, we further split up the univariate series along the time dimension to create single entities of different granularity, which we then use for context creation. We normalize the time dimension of each dataset so that it

fits in the abstract $[-3, 1]$ interval. Furthermore, we apply Z-score normalization, with 2 standard deviations, to the values of each univariate time series.

The specifics of each dataset are presented in the following sections. We reference the original sources of the datasets. However, practically we obtained the actual files from the ForecastPFN repository [17, 2]

C.3.1 Illness

Illness is a dataset of influenza-like illness patients in the United States. It reports patients data in a weekly time granularity, from 1997 to 2024. [1]

During pre-processing, we create files for each column of the dataset and split them along the time dimension, with a monthly periodicity.

We define a sequence length of 160 equidistant intervals, of which the last 25% are used as the prediction target. We use a rolling window over the dataset, with a stride of 1.

We hand-picked 4 windows of the historic series as context examples and kept 1 as held-out starting from forecast date 01-01-2018, which we evaluate the zero-shot performance on.

Context	Held-out
ILITOTAL 2008-2012	ILITOTAL 2018-2022
ILITOTAL 2013-2017	
TOTAL_PATIENTS 2008-2012	
TOTAL_PATIENTS 2013-2017	

C.3.2 EttH1 & EttH2

The ETT (Electricity Transformer Temperature) dataset is an electricity power deployment dataset. The data is reported both hourly and minute-wise, from 2016-07-01 to 2018-06-26. The dataset reports two different series, ETT1, and ETT2, corresponding to two different transformer stations, where the data was recorded [65].

We experiment on the hourly series but aggregate the data monthly and create univariate time series out of each column. Following the dataset's original directions, we use the OT column as held-out, on which we evaluate the zero-shot performance of the model.

We define a sequence length of 240 equidistant intervals, of which the last 25% are used as targets. We use a rolling window over each time series with a stride of 10.

We run 2 separate experiments for this dataset, one for each transformer station series. We change both the held-out series and context for each experiment.

- Experiment 1: ETTh1
  We provide a context dimension of 14 and leave one held-out time series.

Context	Held-out
ETTh1 HUFL 2017/01 - 2017/05	ETTh1 OT 2018/01 - 2018/05
ETTh1 HULL 2017/01 - 2017/05	
ETTh1 LUFL 2017/01 - 2017/05	
ETTh1 LULL 2017/01 - 2017/05	
ETTh1 MUFL 2017/01 - 2017/05	
ETTh1 MULL 2017/01 - 2017/05	
ETTh1 OT 2017/01 - 2017/05	
ETTh2 HULL 2017/01 - 2017/05	
ETTh2 LUFL 2017/01 - 2017/05	
ETTh2 LULL 2017/01 - 2017/05	
ETTh2 MUFL 2017/01 - 2017/05	
ETTh2 MULL 2017/01 - 2017/05	
ETTh2 OT 2017/01 - 2017/05	

- Experiment 2 - ETTh2:
  We provide a context dimension of 4 and leave one held-out time series.

Context	Held-out
ETTh1 HUFL 2017/01 - 2017/05	ETTh2 OT 2018/01 - 2018/05
ETTh1 OT 2017/01 - 2017/05	
ETTh2 HUFL 2017/01 - 2017/05	
ETTh2 OT 2017/01 - 2017/05	

C.3.3 Traffic

Traffic is a dataset reporting freeway congestion in California, USA. We used the data from [17], who originally sourced it from [11]. The data is aggregated daily and consists of 860 numerical columns (named 1-860), plus a target column (OT).

We aggregate the data monthly and create univariate time series for each of the columns.

We define a sequence length of 240 equidistant intervals, of which the last 25% are used as targets. We use a rolling window over each time series with a stride of 1.

We provide a context dimension of 8 and leave two held-out time series.

Context	Held-out
360 2016/11 - 2017/05	360 2017/11 - 2018/05
360 2016/10 - 2017/04	360 2017/08 - 2018/02
293 2016/11 - 2017/05	
293 2016/10 - 2017/04	
710 2016/11 - 2017/05	
710 2016/10 - 2017/04	
405 2016/11 - 2017/05	
405 2016/10 - 2017/04	

C.3.4 ECL

ECL (Electricity Consuming Load) [52] reports electricity consumption in Kwh with an hourly frequency from 2016-07-01 to 2019-07-02. The data consists of 320 numerical columns (named 0-319), plus a target column (OT)

We aggregate the data daily and create univariate time series for each of the columns.

We define a sequence length of 240 equidistant intervals, of which the last 25% are used as targets. We use a rolling window over each time series with a stride of 10.

We provide a context dimension of 15 and leave two held-out time series.

Context	Held-out
OT 2019/01/01 - 2018/01/14	OT 2019/05/01 - 2018/05/14
OT 2019/01/07 - 2018/01/20	OT 2019/04/01 - 2018/04/14
OT 2019/01/17 - 2018/01/30	
OT 2019/02/01 - 2019/02/14	
OT 2019/02/07 - 2019/02/20	
OT 2019/02/17 - 2019/03/02	
OT 2019/03/01 - 2019/03/14	
OT 2019/03/07 - 2019/03/20	
OT 2019/03/17 - 2019/03/30	
OT 2017/04/01 - 2017/04/14	
OT 2017/04/07 - 2017/04/20	
OT 2017/04/17 - 2017/04/30	

C.4 Training & Tuning

Please consider the following training and tuning details:

- We use a Cosine Annealing With Decay and Warm restarts Learning rate schedule. Base learning rate is 9e-4 and the scheduler parameters consist of a decay of 0.96 and a T0 of 9.

- We train with a linear warmup of 95 epochs for JEPA-EMA decay and weight decay. Increasing the former from 0.9952 to 1.0 and the latter from 1.77e-4 to 4.9e-2.

- We tune all of the above hyperparameters with Optuna [3] in the 3 runs, spanning a total of 216 hours.

- We apply MUP [59], which allows us to tune a smaller model and zero-shot transfer the hyperparameters we found. This also proved essential for training stability. MUP also provides us with the MUP-AdamW optimizer [59, 39, 33], which was the optimizer in all experiments.

- All the variables in the bullets below were not tuned but hand-picked by either trial and error or expert knowledge.

- We apply TF32 quantization but no mixed-precision training since this gave stability issues

- For the final model we train with a batch size of 32, a context size of 14, a history of 180, horizon of 60 and held-out size of 2.

- For system identification we multi-target regress to 10 simulation parameters, unit-normalized. Specifically, these variables and normalization scales are:
  - Annual frequency scale: unit-normalized
  - Monthly frequency scale unit-normalized
  - Weekly frequency scale: unit-normalized
  - Trend linear: unit-normalized
  - Trend exponential: log-unit-normalized
  - Offset linear: unit-normalized
  - Offset exponential: unit-normalized
  - Noise scale: log-unit-normalized
  - Resolution: log-unit-normalized

- Since we have a synthetic dataset, we have no natural end of an epoch. We elect to choose a 250-batch epoch before updating schedules.

- We map our training data to an abstract time domain of $[-3, 1]$, with the forecast moment at the origin.

- We define 100 bins on the abstract $[-3.5, 3.5]$ range, as the output space for the decoder.

- Model-width is set at 512 neurons for the final model and 128 neurons for tuning. Corresponding depths are:
  - Embedder: 8 layers
  - Predictor: 3 layers
  - SI-head: 2 layers
  - Decoder: 3 layers

- On top of the compute documented in Section 4, which indicates the compute required to train one seed of the final model, we additionally used more compute for experiments in the discovery phase. How much is unfortunately not something we have kept track of.

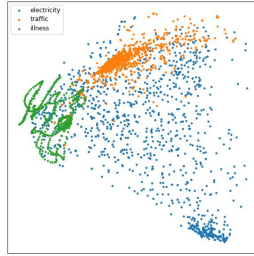Figure 12: PCA plot of fixed-length summary embeddings grouped by domain
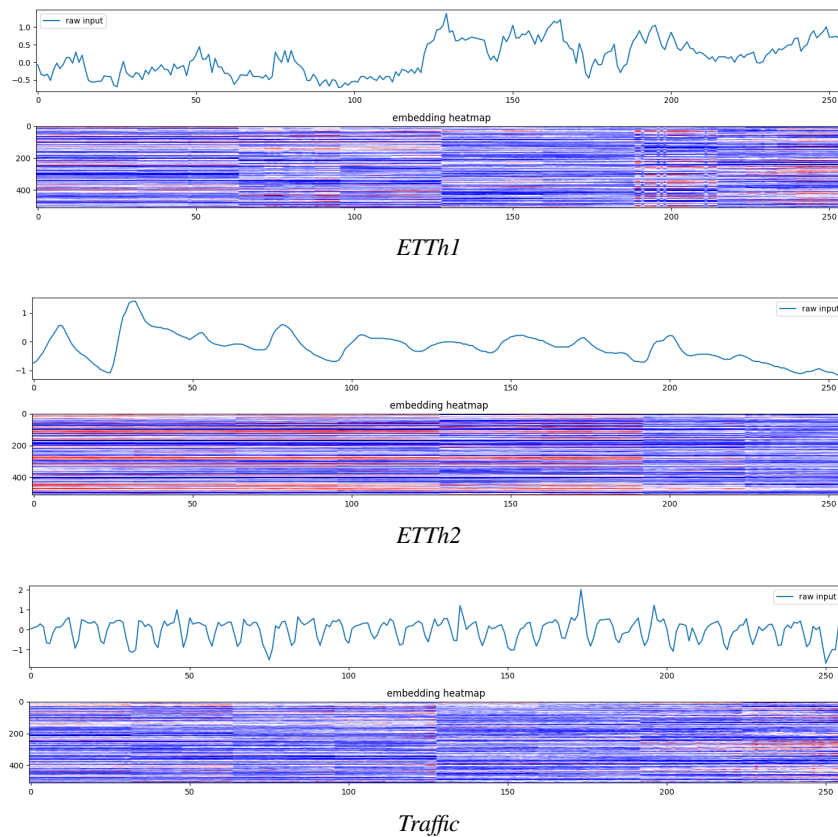
D Latent Space Visualised

ETTh1

ETTh2

Traffic

Figure 13: Additional per-step time series embeddings

E Additional results

E.1 UCR [20] Accuracy by Dataset

Table 4: UCR scores per dataset: A-F

UCR Datasets	Our work	TS2Vec
ACSF1_TEST	37.00%	41.00%
Adiac_TEST	2.05%	2.05%
AllGestureWiimoteX_TEST	29.14%	25.14%
AllGestureWiimoteY_TEST	25.00%	17.86%
AllGestureWiimoteZ_TEST	22.86%	16.43%
ArrowHead_TEST	46.29%	41.71%
BME_TEST	54.00%	46.67%
Beef_TEST	50.00%	40.00%
BeetleFly_TEST	60.00%	85.00%
BirdChicken_TEST	60.00%	75.00%
CBF_TEST	53.33%	47.56%
Car_TEST	21.67%	21.67%
Chinatown_TEST	60.06%	76.38%
ChlorineConcentration_TEST	53.26%	53.26%
CinCECGTorso_TEST	29.06%	25.58%
Coffee_TEST	75.00%	82.14%
Computers_TEST	56.40%	66.40%
CricketX_TEST	29.23%	13.85%
CricketY_TEST	24.87%	17.44%
CricketZ_TEST	29.49%	14.36%
Crop_TEST	38.66%	32.28%
DiatomSizeReduction_TEST	30.07%	30.07%
DistalPhalanxOutlineAgeGroup_TEST	67.63%	46.76%
DistalPhalanxOutlineCorrect_TEST	58.33%	58.33%
DistalPhalanxTW_TEST	58.27%	30.22%
DodgerLoopDay_TEST	23.75%	37.50%
DodgerLoopGame_TEST	56.52%	50.00%
DodgerLoopWeekend_TEST	87.68%	89.13%
ECG200_TEST	64.00%	64.00%
ECG5000_TEST	82.69%	87.51%
ECGFiveDays_TEST	49.71%	49.71%
EOGHorizontalSignal_TEST	17.13%	29.83%
EOGVerticalSignal_TEST	21.82%	20.99%
Earthquakes_TEST	74.82%	74.82%
ElectricDevices_TEST	51.87%	54.30%
EthanolLevel_TEST	25.40%	26.40%
FaceAll_TEST	26.63%	42.43%
FaceFour_TEST	44.32%	18.18%
FacesUCR_TEST	27.46%	18.29%
FiftyWords_TEST	22.64%	12.53%
Fish_TEST	14.29%	22.29%
FordA_TEST	76.52%	61.52%
FordB_TEST	65.43%	53.95%
FreezerRegularTrain_TEST	76.70%	75.75%
FreezerSmallTrain_TEST	76.00%	75.86%
Fungi_TEST	60.22%	46.24%

Table 5: UCR scores per dataset: G-R

UCR Datasets	Our work	TS2Vec
GestureMidAirD1_TEST	20.77%	20.00%
GestureMidAirD2_TEST	26.92%	20.77%
GestureMidAirD3_TEST	16.15%	10.00%
GesturePebbleZ1_TEST	40.12%	50.58%
GesturePebbleZ2_TEST	42.41%	31.01%
GunPointAgeSpan_TEST	58.23%	57.91%
GunPointMaleVersusFemale_TEST	62.66%	84.81%
GunPointOldVersusYoung_TEST	52.38%	100.00%
GunPoint_TEST	49.33%	64.67%
Ham_TEST	59.05%	51.43%
HandOutlines_TEST	64.05%	64.05%
Haptics_TEST	22.40%	20.78%
Herring_TEST	59.38%	59.38%
HouseTwenty_TEST	69.75%	71.43%
InlineSkate_TEST	18.18%	18.73%
InsectEPGRegularTrain_TEST	100.00%	100.00%
InsectEPGSmallTrain_TEST	100.00%	100.00%
InsectWingbeatSound_TEST	30.15%	21.26%
ItalyPowerDemand_TEST	61.22%	49.85%
LargeKitchenAppliances_TEST	56.27%	57.60%
Lightning2_TEST	54.10%	54.10%
Lightning7_TEST	30.14%	41.10%
Mallat_TEST	25.54%	12.32%
Meat_TEST	68.33%	53.33%
MedicalImages_TEST	51.45%	51.45%
MelbournePedestrian_TEST	24.52%	62.03%
MiddlePhalanxOutlineAgeGroup_TEST	45.45%	18.83%
MiddlePhalanxOutlineCorrect_TEST	57.04%	57.04%
MiddlePhalanxTW_TEST	46.10%	27.27%
MixedShapesRegularTrain_TEST	59.13%	52.21%
MixedShapesSmallTrain_TEST	48.78%	48.49%
MoteStrain_TEST	87.22%	77.32%
NonInvasiveFetalECGThorax1_TEST	21.63%	1.83%
NonInvasiveFetalECGThorax2_TEST	26.97%	1.83%
OSULeaf_TEST	35.95%	18.18%
OliveOil_TEST	40.00%	40.00%
Overall	51.20%	45.74%
PLAID_TEST	31.10%	24.39%
PhalangesOutlinesCorrect_TEST	61.31%	61.31%
Phoneme_TEST	15.98%	11.29%
PickupGestureWiimoteZ_TEST	38.00%	52.00%
PigAirwayPressure_TEST	5.77%	19.71%
PigArtPressure_TEST	4.81%	25.96%
PigCVP_TEST	5.29%	46.63%
Plane_TEST	22.86%	9.52%
PowerCons_TEST	87.22%	85.56%
ProximalPhalanxOutlineAgeGroup_TEST	82.44%	48.78%
ProximalPhalanxOutlineCorrect_TEST	68.38%	68.38%
ProximalPhalanxTW_TEST	63.90%	35.12%
RefrigerationDevices_TEST	39.20%	54.40%
Rock_TEST	46.00%	34.00%

Table 6: UCR scores per dataset: S-Z

UCR Datasets	Our work	TS2Vec
ScreenType_TEST	45.33%	40.80%
SemgHandGenderCh2_TEST	74.33%	58.83%
SemgHandMovementCh2_TEST	30.89%	35.11%
SemgHandSubjectCh2_TEST	37.11%	35.56%
ShakeGestureWiimoteZ_TEST	54.00%	64.00%
ShapeletSim_TEST	50.56%	87.78%
ShapesAll_TEST	28.00%	42.67%
SmallKitchenAppliances_TEST	40.53%	55.47%
SmoothSubspace_TEST	57.33%	78.00%
SonyAIBORobotSurface1_TEST	59.73%	42.93%
SonyAIBORobotSurface2_TEST	78.07%	61.70%
StarLightCurves_TEST	82.93%	84.74%
Strawberry_TEST	64.32%	64.32%
SwedishLeaf_TEST	31.68%	8.48%
Symbols_TEST	55.78%	17.39%
SyntheticControl_TEST	50.33%	77.33%
ToeSegmentation1_TEST	70.61%	65.79%
ToeSegmentation2_TEST	80.77%	80.77%
Trace_TEST	65.00%	19.00%
TwoLeadECG_TEST	49.96%	49.96%
TwoPatterns_TEST	31.62%	25.87%
UMD_TEST	49.31%	50.00%
UWaveGestureLibraryAll_TEST	51.84%	12.37%
UWaveGestureLibraryX_TEST	57.31%	22.28%
UWaveGestureLibraryY_TEST	44.89%	20.38%
UWaveGestureLibraryZ_TEST	52.07%	31.38%
Wafer_TEST	89.21%	89.21%
Wine_TEST	50.00%	50.00%
WordSynonyms_TEST	29.31%	21.94%
WormsTwoClass_TEST	62.34%	57.14%
Worms_TEST	46.75%	42.86%
Yoga_TEST	52.97%	53.57%

End of the Appendix.